Inorganic Chemistry

Article

pubs.acs.org/IC

Cyclometalated Iridium(III) Complexes Containing Hydroxide/Chloride Ligands: Isolation of Heterobridged Dinuclear Iridium(III) Compounds Containing μ-OH and μ-Pyrazole Ligands

Vadapalli Chandrasekhar,*[,†] Bani Mahanti,[†] Priyanka Bandipalli,[‡] and Kotamarthi Bhanuprakash*[,‡]

[†]Department of Chemistry, Indian Institute of Technology Kanpur, Kanpur 208 016, India

[‡]Inorganic and Physical Chemistry Division, Indian Institute of Chemical Technology, Hyderabad 500 607, India

Supporting Information

ABSTRACT: The reaction of the cyclometalated chloro-bridged iridium(III) dimers $[(ppy)_2\ Ir(\mu\text{-}Cl)]_2$ (ppyH = 2-phenyl pyridine) and $[(tpy)_2Ir(\mu\text{-}Cl)]_2$ (tpyH = 2-*p*-tolylpyridine) with 3,5-diphenylpyrazole (Ph_2PzH) in the presence of sodium methoxide resulted in the formation of heterobridged dimers $[(ppy)_2Ir(\mu\text{-}OH)(\mu\text{-}Ph_2Pz)Ir(ppy)_2]$ (**1**) and $[(tpy)_2Ir(\mu\text{-}OH)(\mu\text{-}Ph_2Pz)Ir(tpy)_2]$ (**2**). Interestingly, the reaction of $[(ppy)_2Ir(\mu\text{-}Cl)]_2$ with 3(5)-methyl-5(3)-phenylpyrazole (PhMePzH) afforded both a heterobridged dimer, $[(ppy)_2Ir(\mu\text{-}OH)(\mu\text{-}PhMePz)Ir(ppy)_2]$ (**3**), and the monomer $[(ppy)_2Ir(PhMePz)Cl]$ (**4**). The compound $[(ppy)_2Ir(PhMePz)OH]$ (**5**) containing a terminal OH was obtained in a hydrolysis reaction involving **4**, sodium methoxide, and PhMePzH. Complexes **1**−**5** were characterized by X-ray crystallography and electrospray ionization high-resolution mass spectrometry. All of the complexes are luminescent at room temperature in their dichloromethane solutions. The luminescence of the dinuclear complexes is characterized by a single structureless band centered at λ_{max} = 550 nm (**1** and **3**) and 546 nm (**2**). The emission spectra of the mononuclear complexes **4** and **5** display vibronic structures with their λ_{max} values at 497 nm (**4**) and 513 nm (**5**). In each case, the main emission bands are accompanied by shoulder bands at 526 (**4**) and 534 nm (**5**). The quantum yields, calculated with reference to $[Ir(ppy)_2(bpy)]PF_6$ (Φ_{CH_3CN} = 0.0622), range from 0.11 to 0.17 for the dinuclear complexes and 0.045 to 0.048 for the mononuclear complexes. The lifetimes of the emission are in the microsecond region, suggesting the phosphorescent nature of the emission. Density functional theory (DFT) and time-dependent DFT calculations were performed on complexes **1** and **4** in the ground state to gain insight into the structural, electronic, and photophysical properties. Electrochemical studies on complexes **1**−**3** showed the presence of two consecutive one-electron-oxidation processes, assigned as the stepwise oxidation of the two Ir^{III} centers, i.e., Ir^{III}−Ir^{III}/Ir^{III}−Ir^{IV} and Ir^{III}−Ir^{IV}/Ir^{IV}−Ir^{IV} couples, respectively. The monomers displayed single-oxidation peaks. No reduction process was observed within the solvent cathodic potential limit.

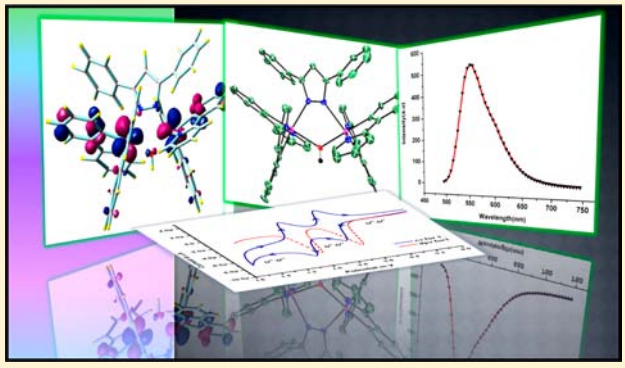

INTRODUCTION

Pyrazole and ligands based on the pyrazole motif are ubiquitous and are among the most widely used ligands in coordination and organometallic chemistry.[1−4] One of the reasons for this widespread utility is the versatile and adaptable coordination modes that are exhibited by these ligands (Chart S1, Supporting Information).[1,4,5] Another reason is the ready tunability of the electronic and steric features of the ligands by relatively simple synthetic strategies.[6−9] A third reason is that the multisite coordination ligands that contain multiple pyrazole units or pyrazole unit(s) along with other coordinating groups are also readily accessible.[10,11] We have been examining pyrazole-based ligands for their ability to function as bridging ligands in main-group chemistry and have reported several multinuclear organotin compounds including coordination polymers.[12,13] In view of this, we were interested in exploring the bridging-coordination chemistry of pyrazole ligands in other situations.

Cyclometalated organometallic iridium(III) compounds have been of considerable interest in recent years in view of their excellent photophysical properties and particularly their potential utility as phosphorescent dopants in organic light-emitting diodes.[14−17] Most of the known compounds, however, are mononuclear, and relatively less attention seems to have been given to higher-nuclearity compounds[18−29] probably because of the synthetic difficulties involved,[20,28] resulting in compounds with low yields; in some cases, unidentified complexes or a mixture of isomers have been obtained.[20,28] We have recently initiated a program to build di- and multinuclear cyclometaled iridium(III) complexes. We have

Received: April 4, 2012
Published: September 26, 2012

Scheme 1. Synthesis of Complexes 1−4

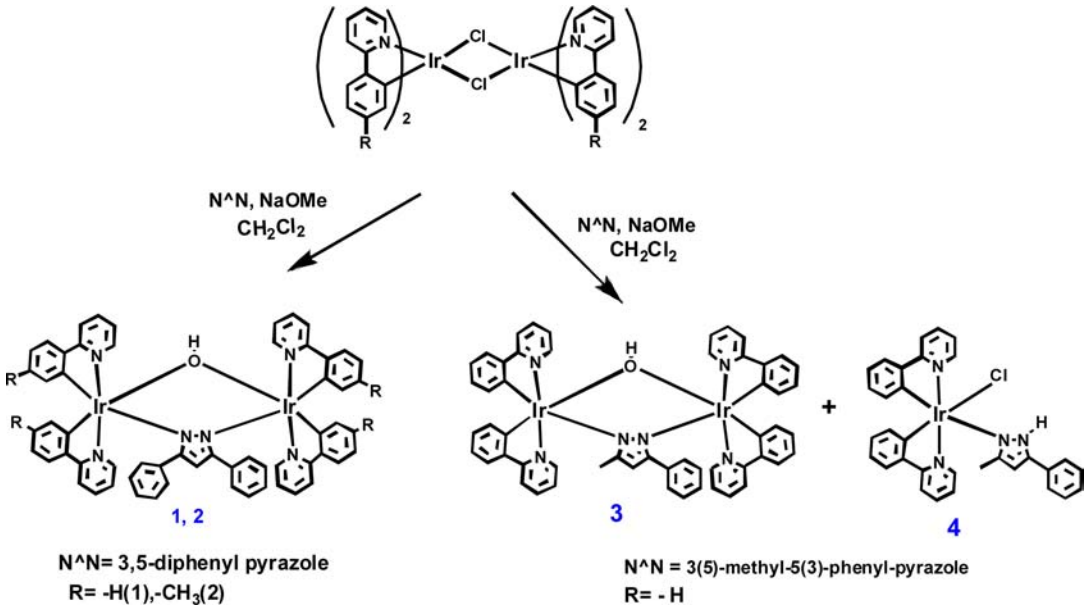

Scheme 2. Synthesis of Complex 5

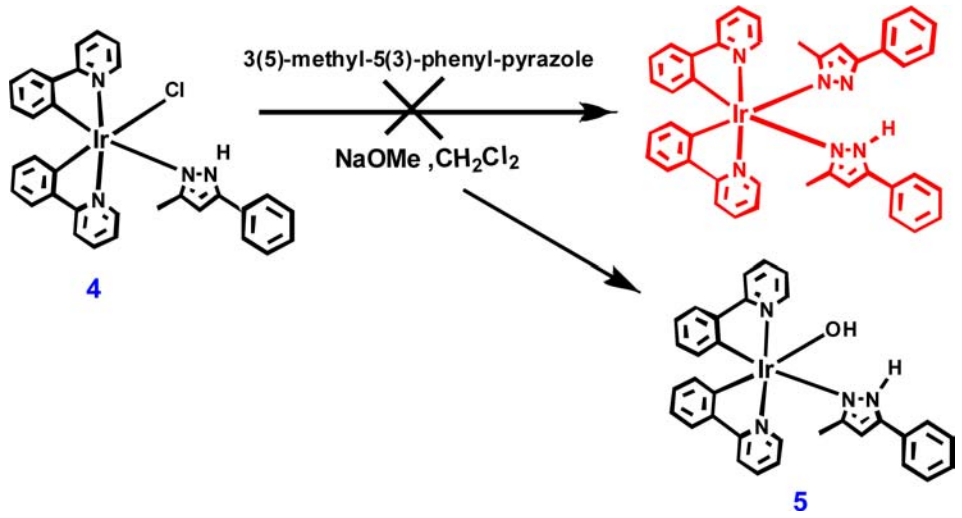

used various types of bridging ligands and have achieved synthesis of the di- and trinuclear derivatives.[23,30−32] In view of the fact that pyrazole ligands can be readily tuned in terms of both their electronic and steric features and also because they have earlier found use in cyclometalated iridium(III) compounds,[33−35] we were interested in examining whether pyrazole ligands can be employed as bridging ligands to assemble dinuclear derivatives. We employed different types of pyrazole ligands whose steric bulk was modulated by varying the number and nature of substituents on the pyrazole backbone (in their 3 and 5 positions). We reasoned that it would be difficult to accommodate two sterically hindered pyrazole ligands in a mononuclear compound. In such a situation, the formation of dinuclear compounds, mediated by the bridging coordination action of the pyrazole ligand, would be feasible. Accordingly, in this paper, we report the first examples of heterobridged (pyrazole- and hydroxide-bridged) cyclometalated iridium(III) dimers, $[(ppy)_2Ir(\mu\text{-}OH)(\mu\text{-}Ph_2Pz)Ir(ppy)_2]$ (**1**), $[(tpy)_2Ir(\mu\text{-}OH)(\mu\text{-}Ph_2Pz)Ir(tpy)_2]$ (**2**), and $[(ppy)_2Ir(\mu\text{-}OH)(\mu\text{-}PhMePz)Ir(ppy)_2]$ (**3**), where ppyH = 2-phenylpyridine, tpyH = 2-*p*-tolylpyridine, Ph_2PzH = 3,5-diphenylpyrazole, and PhMePzH = 3(5)-methyl-5(3)-phenyl-pyrazole. Interestingly, employing PhMePzH, we could also isolate monomers $[(ppy)_2Ir(PhMePz)Cl]$ (**4**) and $[(ppy)_2Ir(PhMePz)OH]$ (**5**), whose photophysical properties were different from those of **3**. All of the complexes are found to be emissive at room temperature. The synthesis, structures, photophysical properties, and theoretical studies of these novel iridium(III) compounds are presented herein.

RESULTS AND DISCUSSION

Synthesis. The cyclometalated chloro-bridged iridium(III) dimers $[(ppy)_2Ir(\mu\text{-}Cl)]_2$ and $[(tpy)_2\ Ir(\mu\text{-}Cl)]_2$ were prepared by using the Nonoyama protocol.[36] Subsequent reactions of these iridium(III) dimers with sodium methoxide, followed by reaction with Ph_2PzH, afforded the heterobridged dimers **1** and **2** in very good yields (Scheme 1). The presence of adventitious moisture in the solvent presumably leads to the replacement of

dx.doi.org/10.1021/ic300694m | *Inorg. Chem.* 2012, 51, 10536−10547

a bridging μ-OMe group by a μ-OH group. Evidence for the formation of compounds containing μ-OMe groups was found earlier.[37] Further, in a reaction involving $[(ppy)_2Ir(\mu\text{-}Cl)]_2$ and Ph_2PzH in the presence of NaOH, we were able to isolate compound **1** (Scheme S1, Supporting Information). As described herein, in other reactions, we have isolated cylometalated iridium(III) compounds containing terminal chloride and hydroxide ligands.

Under the same experimental conditions as those used for the preparation of **1** and **2**, the reaction of $[(ppy)_2Ir(\mu\text{-}Cl)]_2$ with PhMePzH afforded a mixture of products that could be separated by column chromatography using ethyl acetate and petroleum ether [60−80 °C; 10:90 (v/v)], affording **3** (orange in color, heterobridged dimer) and **4** (yellow in color, heteroleptic monomer) (Scheme 1). The ^{1}H NMR spectrum of **4** showed a sharp low-field singlet at δ 13.69, indicating the presence of a strong hydrogen bond (N−H···Cl). Such downfield shifts have been reported previously for protons involved in hydrogen bonding.[34]

The reaction of **4** with PhMePzH in the presence of the base NaOMe afforded **5**, which contains a terminal Ir−OH bond (Scheme 2). Thus, we have been able to isolate dimeric compounds containing μ-pyrazole and μ-OH bridges (compounds **1**−**3**) as well as mononuclear compounds containing terminal Ir−Cl (**4**) and Ir−OH (**5**) groups. The molecular structures of all of these complexes (**1**−**5**) were established by single-crystal X-ray analysis as described later.

The IR spectra of **1**−**3** showed a broad band at 3450 cm^{-1} corresponding to the μ-OH group;[38] such a broad band is also found for **5** (3442 cm^{-1}), which contains a terminal OH group. This feature is absent in **4**. The solution stability of compounds **1**−**5** was probed by electrospray ionization high-resolution (ESI-HR) mass spectrometry. ESI-HR mass spectra of **1**−**3** showed intense peaks due to $[M - OH]^+$ and $[M - OH + CH_3CN]^+$ in addition to the molecular ion peaks (Figure 1 for **1** and Figures S1, Supporting Information, for **2** and **3**). ESI-HR mass spectra of **4** and **5** showed peaks due to $[M - Cl]^+$ and $[M - OH]^+$ respectively.

Molecular Structures of 1−5. The molecular structures of **1**−**5** were determined by X-ray crystallographic analysis. ORTEP diagrams of the dinuclear derivatives **1**−**3** are shown in Figure 2, while those of the mononuclear derivatives **4** and **5** are given in Figure 3. Crystallographic data for all of the compounds are summarized in Tables 1 and 2. Selected bond parameters for all of the complexes are given in the Supporting Information (Tables S1−S5).

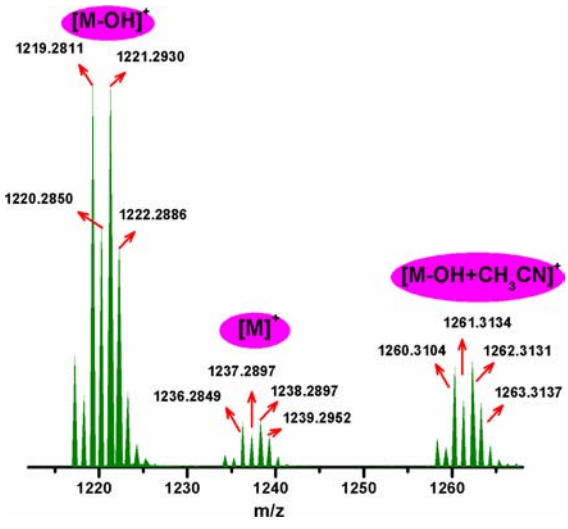

Figure 1. ESI-HR mass spectrum of **1** showing $[M - OH]^+$, $[M]^+$, and $[M - OH + CH_3CN]^+$ peaks.

Complexes **1**−**3** are neutral compounds and are dinuclear cyclometalated iridium(III) compounds containing two different types of anionic bridging groups (μ-OH and μ-η^1:η^1-Pz). The pyrazole ligand is known to bind to transition-metal ions in many ways (Chart S1, Supporting Information).[1,2,4] The mode of binding observed in **1**−**3** corresponds to the μ-η^1:η^1 mode observed with anionic pyrazolate ligands.[1,2,4] Although pyrazole ligands have been known to be involved as bridging ligands in some diiridium complexes,[39,40] to the best of our knowledge, **1**−**3** represent the first examples of dinuclear iridium compounds containing two different bridging ligands. The heteroleptic bridging coordination mode present in **1**−**3** results in the formation of a puckered five-membered $[Ir_2N_2O]$ ring. Compounds **4** and **5** are neutral heteroleptic monomers containing one neutral pyrazolate ligand binding in a η^1 manner (Chart S1, Supporting Information).

In all of the complexes described herein, a distorted octahedral geometry is present around the metal center. The N atoms of the cyclometalating ligands occupy trans positions ($Ir-N_{pyridyl}$ bond), while the two C atoms of these ligands are in the cis orientation, thus retaining the coordination mode and geometry present in the precursor complexes $[(ppy)_2Ir(\mu\text{-}Cl)]_2$ and $[(tpy)_2Ir(\mu\text{-}Cl)]_2$. Such a geometrical arrangement is also well-known in many other cyclometalated iridium(III) complexes.[19,20,22]

An inspection of the bond parameters of **1**−**3** reveals that the Ir−N distances involving the bridging pyrazole ligand are slightly longer [2.176(11)−2.196(7) Å] than those involving the cyclometalating ligand (C^N ligand) [2.018(11)−2.061(11) Å]; the strong trans influence of the metalated C atom of the C^N ligand is presumably responsible for the longer Ir−N distances of the bridging pyrazole ligand. The trans N−Ir−N bond angles are approximately 172° and are similar to those reported for this class of complexes. In these dimeric complexes, the Ir−O bond length involving the μ-OH group varies in a narrow range from 2.141(6) to 2.155(8) Å and can be compared to previously reported iridium(III) dihydroxo-bridged complexes. The Ir−O−Ir bond angles vary between 122.3(4) to 124.1(3)° and are not unexceptional.[38] The nonbonding Ir···Ir distances (3.765, 3.781, and 3.772 Å) are in ranges similar to those found in literature precedents [3.803 and 3.770(3) Å].[40]

The metric parameters of the monomeric complexes **4** and **5** are unexceptional and are similar to those found in other cyclometalated iridium(III) compounds.[34] The Ir−Cl bond distance in **4** is 2.492(13) Å. The $Ir-N_{Pz}$ distance in **4** is 2.211(4) Å. These data may be compared with those found in **1**−**3**. The Ir−O bond distance found in **5** (contains a terminal Ir−OH bond) is 2.377(10) Å, which is longer than that found in **1**−**3**, where the OH group is a bridging ligand.

Photophysical Properties. To examine the photophysical properties of **1**−**5**, the room temperature absorption and emission spectra were recorded in a 10^{-5} M dichloromethane solution, the results of which are compiled in Table 3.

Dinuclear complexes **1**−**3** exhibit intense absorption in the ultraviolet (UV) region at around 260−300 nm ($\varepsilon > 10^4$ M^{-1} cm^{-1}), which is due to π−π* transitions on the coordinated ligand. Similar absorption features are also seen for the

dx.doi.org/10.1021/ic300694m | Inorg. Chem. 2012, 51, 10536−10547

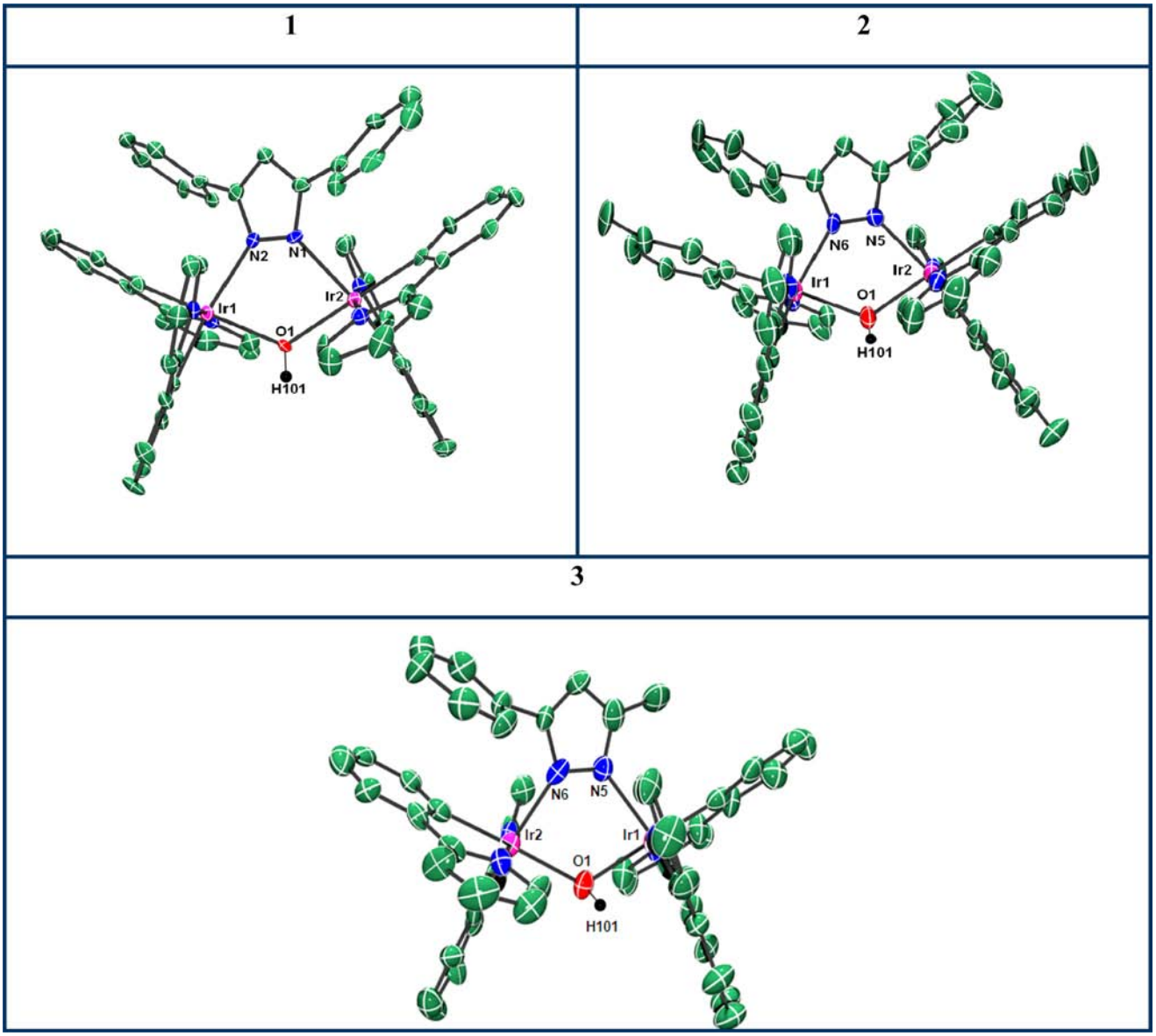

Figure 2. *ORTEP* diagrams of **1**–**3** with thermal ellipsoids at the 50% probability limit (H atoms, except the bridging ones, and solvent molecules are omitted for clarity).

mononuclear complexes **4** and **5** (Figure 4 and Table 3). The moderately intense low-energy bands extending up to the visible region in the wavelength range 350–450 nm ($\varepsilon \approx$ 6500–8000 M^{-1} cm^{-1}) are due to spin-allowed ^1ML_CCT, ^1IL_CCT, and $^1L_{OH}L_CCT$ (charge-transfer) transitions, while the spin-forbidden transitions (^3ML_CCT, ^3IL_CCT, and $^3L_{OH}L_CCT$) observed due to a strong spin–orbit coupling effect of the Ir^{III} metal center appear in the range 450–480 nm with a low extinction coefficient ($\varepsilon \approx$ 1600–3000 M^{-1} cm^{-1}). The assignment of these bands was made by time-dependent density functional theory (TDDFT) calculations performed on **1** by using ground-state-optimized geometry (detailed theoretical analyses, DFT as well as TDDFT, are given in the following section and are summarized in Tables S6–S9, Supporting Information). The absorption spectra of all of the dinuclear complexes **1**–**3** show similar profiles and follow the trends previously found in bridged dinuclear complexes.[41,42] From an examination of the spectra, it is clear that the change of the cyclometalating ligand from ppyH (in **1** and **3**) to tpyH (in **2**) as well as the change in the ancillary ligand from Ph_2PzH (in **1** and **2**) to PhMePzH (in **3**) does not have a significant effect on the absorption properties. However, the low-energy bands of the dinuclear complexes **1**–**3** are bathochromically shifted in comparison to those observed for the mononuclear derivatives (see below). We reason that this change is due to the π-donating nature of the bridging ligands, which pushes the electron density toward the Ir^{III} center, thereby increasing the HOMO (highest occupied molecular orbital) energy and thus decreasing the HOMO–LUMO (lowest unoccupied molecular orbital) energy gap. It might be mentioned that a similar shift of the low-energy bands has been found in previously reported dinuclear ruthenium complexes $[\{Ru(bpy)_2\}(\mu\text{-}OMe)_2][PF_6]_2$, $[\{Ru(bpy)_2\}(\mu\text{-}OEt)_2][PF_6]_2$, and $[\{Ru(bpy)_2\}(\mu\text{-}OMe)(\mu\text{-}Pyz)]^{2+}$ in comparison to a mononuclear complex, $[Ru(bpy)_3]^{2+}$.[41,42]

The absorption characteristics of the mononuclear complexes **4** and **5** are similar to those of **1**–**3** and also to analogous compounds reported in the literature (Figure 4 and Table 3).

dx.doi.org/10.1021/ic300694m | *Inorg. Chem.* 2012, 51, 10536–10547

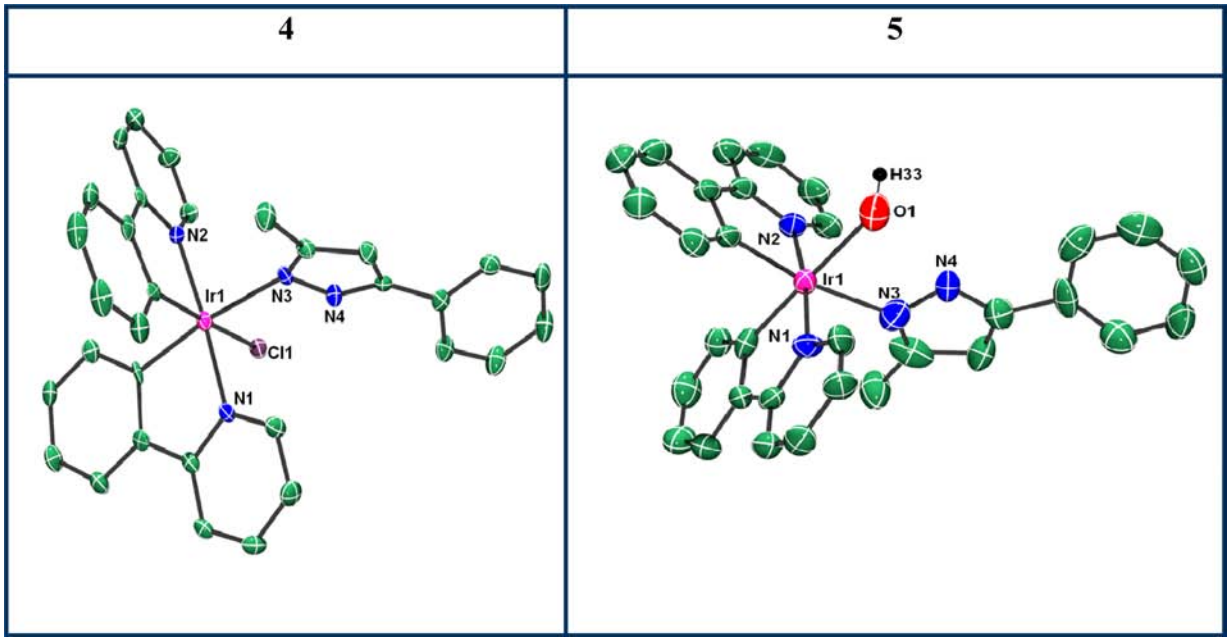

Figure 3. *ORTEP* diagrams of **4** and **5** with thermal ellipsoids at the 50% probability limit (H atoms and solvent molecules are omitted for clarity).

Table 1. Crystallographic Data of Compounds 1−3

parameters	1	2	3
formula	$C_{62}H_{48}Cl_6Ir_2N_6O_2$	$C_{64}H_{54}Cl_2Ir_2N_6O$	$C_{57}H_{52}Cl_2Ir_2N_6O_3$
fw	1506.16	1378.43	1324.35
cryst syst	orthorhombic	monoclinic	orthorhombic
space group	*Pbca*	$P2_1/c$	*Pbca*
a/Å	18.2538(18)	25.744(5)	18.312(3)
b/Å	25.024(2)	11.615(2)	23.253(4)
c/Å	24.809(2)	20.613(4)	25.194(4)
α/deg	90	90	90
β/deg	90	90.561(3)	90
γ/deg	90	90	90
V/Å^3	11332.3(19)	6164(2)	10728(3)
Z	8	4	8
calcd density/(g cm^{-3})	1.766	1.485	1.640
abs coeff/mm^{-1}	5.026	4.444	5.105
F(000)	5872	2704	5184
θ range for data collection/deg	1.98−25.00	1.98−26.00	4.10−25.03
reflns collected	56189	12100	53320
indep reflns	9960 [*R*(int) = 0.0870]	12100 [*R*(int) = 0.000]	9423 [*R*(int) = 0.1631]
param	702	684	649
GOF on F^2	1.091	1.051	1.015
final *R* indices	0.0473	0.0506	0.0675
R indices (all data)	0.0692	0.0608	0.1215

All of the complexes (**1**−**5**) are luminescent at room temperature in their dichloromethane solutions. In contrast to the absorption spectra, the emission spectra of the dinuclear and mononuclear complexes differ significantly. The calculated HOMO−LUMO gap (Table S10, Supporting Information; PBE0/LANL2DZ/6-31G(d) level for all) is the highest for **4** (4.01 eV), followed by **5** (3.83 eV), and is the lowest in **1** and **3** (3.73 and 3.70 eV). As expected from the energy gaps, the emission follows the order **4** (497 nm) < **5** (513 nm) <**1** ≈ **3** (550 nm). Substitutions at different positions perturb the HOMO energy to a greater extent (varying from −4.95 to −5.23 eV) compared to the LUMO energy (from −1.17 to −1.25 eV).

The luminescence of the dinuclear complexes is characterized by a single structureless band centered at λ_{max} = 550 nm (**1** and **3**) and 546 nm (**2**). The hydroxide bridging ligand induces a red shift of 37 nm (in **1** and **3**) and 33 nm (in **2**) compared to the monomer **5**. Emission spectra of the mononuclear complexes **4** and **5** display vibronic-structured bands, with the emission maximum (λ_{max}) observed at 497 nm (**4**) and at 513 nm (**5**). The introduction of the terminal hydroxide group (**5**) in place of a chloride (**4**) results in a bathochromic shift of emission by 16 nm, besides the spectral shape changes from a less resolved vibronic structure (in **4**) to a poorly resolved one (in **5**). In each case, the emission appears as a sharp peak, which is further accompanied by a shoulder at

dx.doi.org/10.1021/ic300694m | *Inorg. Chem.* 2012, 51, 10536−10547

Table 2. Crystallographic Data of Compounds 4 and 5

parameters	4	5
formula	$C_{32}H_{26}ClIrN_4$	$C_{32}H_{27}Ir_4O$
fw	694.22	675.78
cryst syst	triclinic	orthorhombic
space group	$P\bar{1}$	$P2_12_12_1$
a/Å	8.200	9.571(5)
b/Å	12.309	10.490(5)
c/Å	13.904	27.375(5)
α/deg	90.63	90.000
β/deg	93.86	90.000
γ/deg	109.13	90.000
V/Å^3	1322.1	2748(2)
Z	2	4
calcd density/(g cm^{-3})	1.744	1.633
abs coeff/mm^{-1}	5.180	4.889
F(000)	680	1238
θ range for data collection/deg	2.15−25.50	2.25−25.50
reflns collected	7071	39277
indep reflns	4783 [R(int) = 0.0271]	5121 [R(int) = 0.0345]
param	348	348
GOF on F^2	1.027	1.088
final R indices	0.0347	0.0471
R indices (all data)	0.0410	0.0488

Table 3. Photophysical Properties of 1−5 at 25 °C

complex	absorption[a] λ_{max}/nm (×10$^{-4}\varepsilon$/(M^{-1} cm^{-1}))	emission[a] λ_{max}/nm	τ/μs	Φ[b]
1	266 (9.5), 355 (1.3), 414 (0.65), 478 (0.31)	550	3.6	0.17
2	267 (8.7), 356 (1.23), 395 (0.79), 476 (0.30)	546	3.3	0.12
3	264 (7.4), 354 (1.1), 403 (0.77), 479 (0.16)	550	4.2	0.11
4	267 (7.7), 334 (1.3), 355 (0.96), 394 (0.56), 447 (0.28)	497, 526	6.9	0.045
5	261 (7.02), 335 (1.1), 356 (0.91), 401 (0.55), 446 (0.31)	513, 534	4.3	0.048

[a]Absorption and emission (λ_{exc} = 450 nm); spectral data of all of the complexes were recorded in a 10^{-5} M dichloromethane solution at room temperature. [b]Quantum yields are measured with respect to $[Ir(ppy)_2(bpy)]PF_6$ (Φ_{CH_3CN} = 0.0622) in a deaerated solution.

526 nm (**4**) and 534 nm (**5**) (Figure 5). In general, the features of the emission spectra of **4** and **5** are consistent with literature observations.[34,35]

Photoluminescence from iridium(III) complexes is known to originate from either a predominantly ^{3}MLCT state, ^{3}LC, or a mixed ^{3}MLCT/^{3}LC state.[18,22] In order to learn more about the nature of the excited state, we studied the effect of the solvent on emission. Dinuclear and mononuclear compounds show marked differences in their solvatochromic behavior (see Figure S2, Supporting Information). The single structureless band of **1**−**3** does not show any observable shift upon increasing solvent polarity; in contrast, the emission spectra of mononuclear complexes **4** and **5** are slightly red-shifted with an increase in the solvent polarity. An additional feature is that the vibrational structure observed in toluene and dichloromethane is lost upon increasing solvent polarity (acetonitrile and dimethylformamide). These studies, as well as the shapes of the emission spectra, indicate that the excited state possesses a mixed ^{3}MLCT/^{3}LC character in all of the complexes studied.[43,44] However, the influence of the MLCT character becomes more pronounced in polar solvents, particularly for the mononuclear complexes **4** and **5**.

The quantum yields of the complexes were calculated with reference to $[Ir(ppy)_2(bpy)]PF_6$ (Φ_{CH_3CN} = 0.0622)[45] and range from 0.11 to 0.17 for the dinuclear complexes and from 0.045 to 0.048 for the mononuclear complexes. In the literature, it has been recorded that many dinuclear complexes show very low emission quantum yields, in some cases with this being even less than 1%;[19,20,24] there are only a few reports of dinuclear complexes showing high quantum yields.[21,26,27] The quantum yields found for **1**−**3** are comparable to literature precedents.[26,27] The lifetimes of the emission fall in the microsecond region, suggesting the phosphorescent nature of the emission (Table 3).[18,22,29,44]

DFT and TDDFT Studies. DFT and TDDFT studies of transition-metal complexes are being increasingly used to rationalize their observed spectroscopic properties.[46−48] Accordingly, we have performed DFT and TDDFT calculations on **1** (Table S6−S9, Supporting Information) and **4** (Tables S11−S14, Supporting Information) as representative examples to gain insight into the photophysical behavior of the complexes described in this study.

The optimized coordinates and the important molecular orbital compositions of **1** are summarized in Tables S6−S7, Supporting Information, while the isodensity surface plots of some selected molecular orbitals are given in Figure 6. The theoretical calculations reveal that HOMO, HOMO−1, and HOMO−2 are all centered on the Ir atom and the cyclometalating ligand, whereas the LUMO, LUMO+1, and LUMO+2 orbitals are centered mainly on the cyclometalating ligand with negligibly small involvement of the Ir orbitals (<4%). Thus, the overall orbital picture is consistent with that expected for these complexes. In short, 37−40% of the three highest HOMOs are Ir d orbitals, whereas LUMO and the next two unoccupied orbitals are localized on the cyclometalating ligands, which contribute more than 90%. The bridging Ph_2PzH ligand contributes very little electron density to either HOMO or LUMO. However, the bridging hydroxide ligand contributes substantially to the HOMO−2 orbital (20.2%). Even though the structural and spectral properties of all of the dimers are similar, we have, nevertheless, performed similar calculations for complexes **2** and **3** at the PBE0 level. Similar compositions of the molecular orbitals and HOMO−LUMO energy gaps (3.57, 3.59, and 3.64 eV for **1**−**3**, respectively) were obtained (Cartesian coordinates of the optimized geometries, molecular orbital compositions, and isodensity surface plots of some selected molecular orbitals for **2** and **3** are given in Tables S15−S18 and Figure S3, Supporting Information).

TDDFT calculations were employed to understand the nature of the excited states and examine the vertical excitation energies. TDDFT calculations in the framework of the polarizable continuum model (PCM) for a dichloromethane solvent gave good agreement with experimental values despite some deviations (Tables S8 and S9, Supporting Information, summarize the first five singlet and five triplet transitions; Figure 7 displays merged experimental and simulated spectra; all of the singlet transitions are displayed as vertical bars).

The most intense singlet transition in the low-energy region is contributed predominantly by HOMO−2 → LUMO (f = 0.1032 and 426 nm). It is seen that HOMO−2 is composed of Ir d (40.2%) + L_C (34.2%) + OH (20.2%), whereas LUMO is

dx.doi.org/10.1021/ic300694m | Inorg. Chem. 2012, 51, 10536−10547

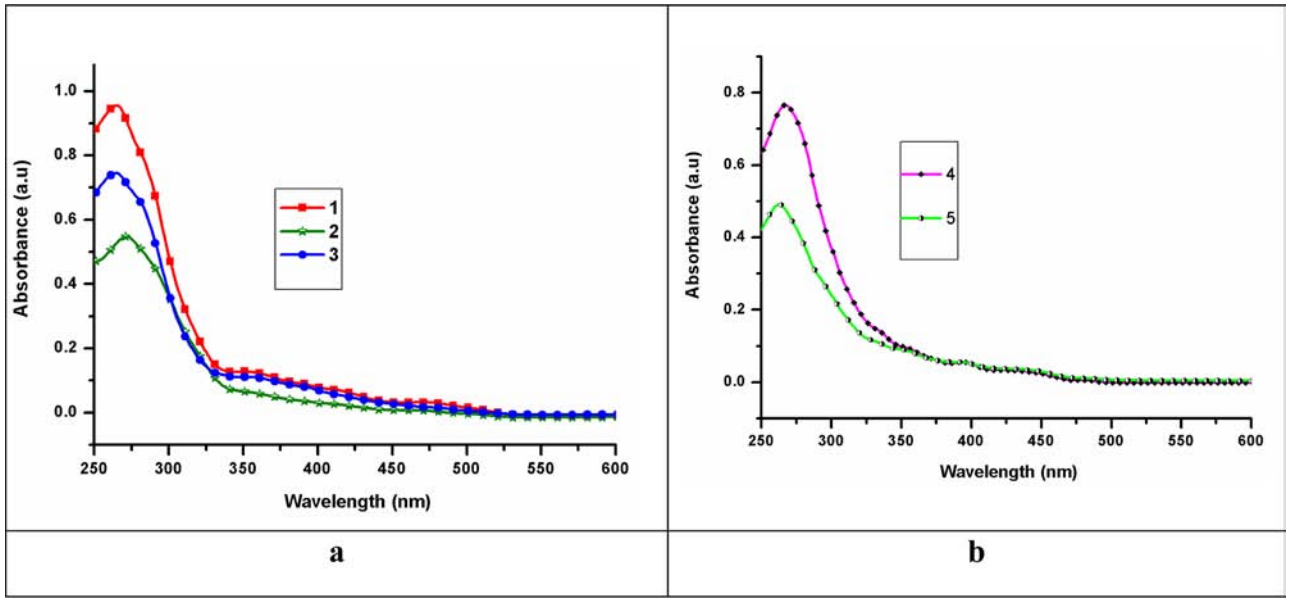

Figure 4. Absorption spectra of (a) **1**−**3** and (b) **4** and **5** in a dichloromethane solution.

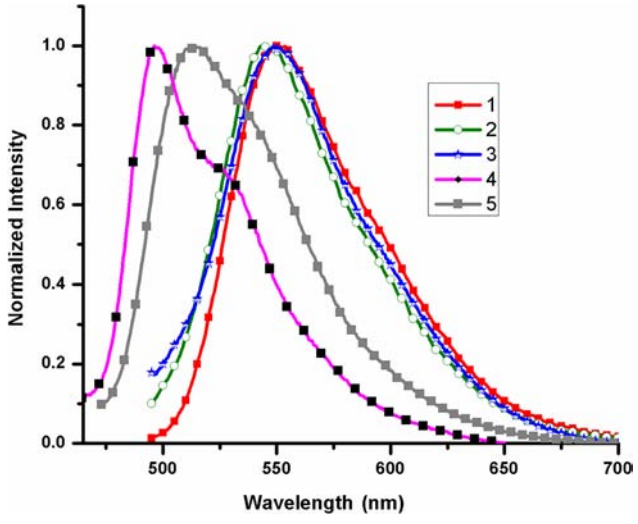

Figure 5. Emission spectra of complexes **1**−**5** in a dichloromethane solution.

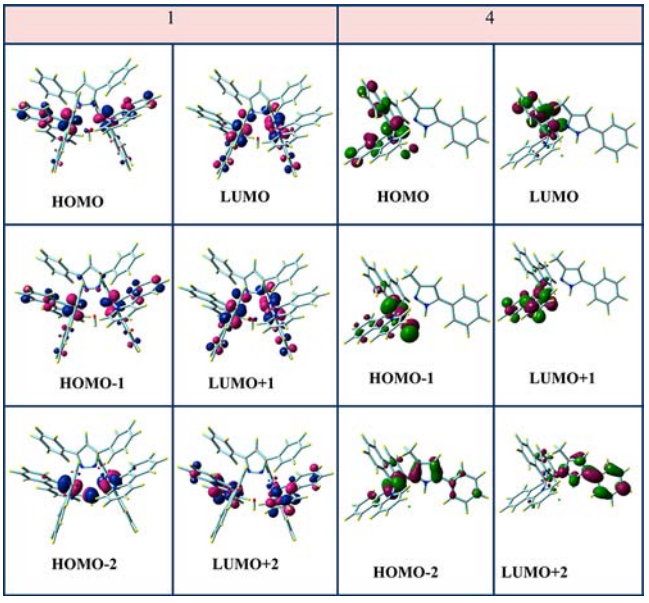

Figure 6. Relevant molecular orbitals of **1** and **4** (isovalue = 0.04) obtained from DFT calculations.

composed of mainly L_C (93.6%) (Table S8, Supporting Information). Thus, the lowest-lying singlet absorption can be attributed to Ir d + L_C + L_{OH} → L_C with mixed ML_CCT, IL_CCT, and $L_{OH}L_CCT$ character. The lowest excitation energies, which are of singlet−triplet character, are also of ML_CCT, IL_CCT, and $L_{OH}L_CCT$ nature (Table S9, Supporting Information). It must be mentioned that the bridging pyrazole ligand is not directly involved in the low-energy excited states; hence, the spectroscopic properties of the complexes remain invariant upon a change of the substituents on this ligand.

The optimized coordinates, important molecular orbital compositions, and isodensity surface plots of some relevant orbitals of **4** are given in Tables S11 and S12, Supporting Information, and Figure 6. Calculations show that LUMO and LUMO+1 are predominantly localized on the cyclometalating ligand (92% contribution), whereas the contribution to LUMO +2 is mainly from the ancillary pyrazole ligand (91% contribution). HOMOs, on the other hand, are composed of contributions from Ir d (50−56%) and the cyclometalating ligand; the terminal chloride contributes 22% electron denisty to the HOMO−1 orbital, whereas the ancillary pyrazole ligand contributes 26.3% electron density to the HOMO−2 orbital.

Tables S13 and S14, Supporting Information, summarize the singlet and triplet excited states for **4** calculated at the PBE0/LANL2DZ/6-31G(d) level using the PCM solvation model. A comparison of the experimental and simulated spectra (considering only the singlet transitions) is reported in Figure 7. The lowest-energy singlet and triplet absorptions can be ascribed as possessing mixed MLCT and ILCT character. The calculated lowest-energy singlet and triplet bands are seen at 392 and 456 nm and are in excellent agreement with the experimentally observed bands at 394 and 447 nm.

The molecular orbital composition and HOMO−LUMO gap of **5** differs from those of **4** (Table S19, Supporting Information; optimized coordinates are given in Table S20,

dx.doi.org/10.1021/ic300694m | *Inorg. Chem.* 2012, 51, 10536−10547

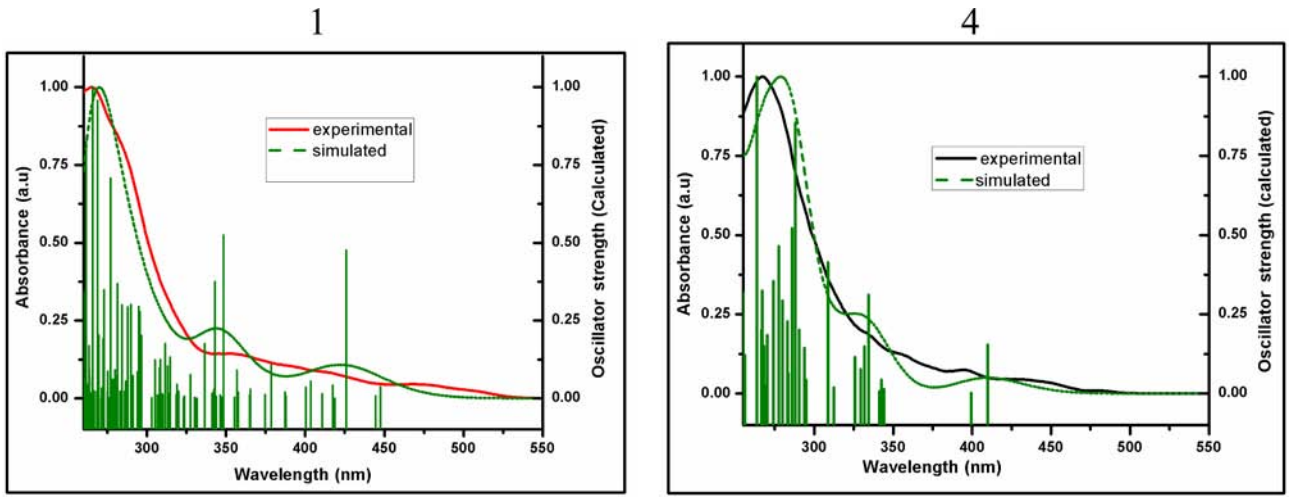

Figure 7. Normalized experimental and calculated UV−vis spectra of **1** and **4**. The singlet excited states are shown as green vertical bars with height equal to the oscillator strength (f). (Calculated spectra were obtained using the program *GAUSSUM-2.1.6.*)

Supporting Information). The three highest HOMOs are composed of 45−63% of Ir d; terminal hydroxide contributes 6% and 9% to the HOMO and HOMO−2 orbitals, ancillary pyrazole contributes 27.6% to the HOMO−1 orbital, while the cyclometalating ligand contributes 39.2%, 12.6%, and 24.8% respectively to the HOMO, HOMO−1, and HOMO−2 orbitals. LUMO, on the other hand, is composed predominantly of the cyclometalating ligand (>90%) with a negligible percentage of other ligands. HOMO of **5** is higher in energy (−5.063 eV) compared to that of **4** (−5.230 eV), whereas LUMO (−1.219 eV in **5** and −1.224 eV in **4**) is nearly invariant. Because the experimental absorption spectrum of **5** is similar to that of **4**, it can be inferred that the low-energy singlet and triplet transitions are of MLCT and ILCT character involving Ir d and the cyclometalating ligand orbitals.

Electrochemical Studies. Cyclic voltammetric studies of **1**−**5** were performed in dry dichloromethane using a 1 mM concentration of the complexes and 0.1 M tetrabutylammonium hexafluorophosphate as the supporting electrolyte. The results obtained are summarized in Table 4. All of the redox events are found to be quasi-reversible.

Table 4. Half-Wave Redox Potentials (vs Ag/AgCl) of 1−5 at 25 °C

complex	$E_1^{1/2,ox}$/V^a (ΔE_p/mV)^b	$E_2^{1/2,ox}$/V^a (ΔE_p/mV)^b
1	0.62 (87)	0.95 (87)
2	0.58 (83)	0.91 (75)
3	0.64 (114)	1.00 (109)
4	1.02 (138)	
5	1.00 (132)	

^{a}Recorded in a dichloromethane solution containing 0.001 M iridium complexes, $E_{1/2} = 1/2(E_{pa} + E_{pc})$, where E_{pa} and E_{pc} are anodic and cathodic peak potentials, respectively. $^b\Delta E_p = E_{pa} - E_{pc}$.

Complexes **1**−**3** show two consecutive one-electron-oxidation processes. A typical voltammogram of **1** along with its differential pulse voltammogram is shown in Figure 8. For this complex, the oxidation peaks appear at 0.62 V (couple 1) and 0.95 V (couple 2); for **2**, these are seen at 0.58 V (couple 1) and 0.91 V (couple 2), whereas for **3**, these events occur at 0.64 V (couple 1) and 1.00 V (couple 2) versus Ag/Ag^+.

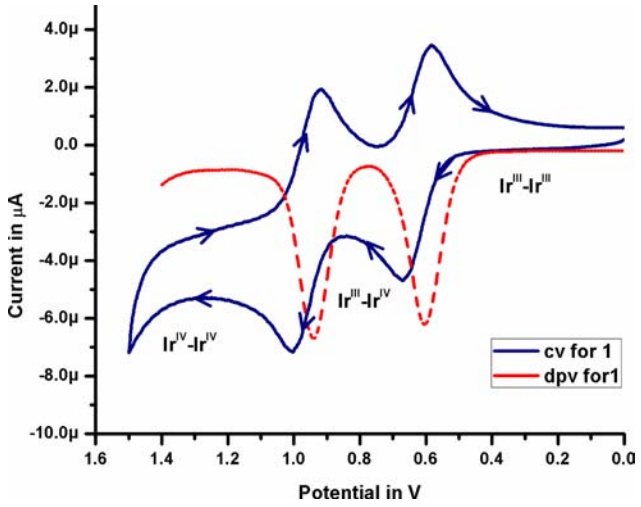

Figure 8. Cyclic voltammogram (blue line) of **1** in dichloromethane at a scan rate of 100 mV s^{-1}. The red line is the differential pulse voltammogram with a step potential of 5 mV and an amplitude of 50 mV.

However, no reduction process was observed within the solvent cathodic potential limit. The oxidation processes are assigned as the stepwise oxidation of the two Ir^{III} centers, i.e., Ir^{III}−Ir^{III}/Ir^{III}−Ir^{IV} and Ir^{III}−Ir^{IV}/Ir^{IV}−Ir^{IV} couples. The presence of two separate sequential redox waves indicates the presence of electronic coupling between the two Ir centers. Differential pulse voltammetry also confirmed the splitting between the waves; the extent of coupling could be assessed by examining their comproportionation constants (K_C). The redox potentials are separated by 332, 338, and 360 mV under the same conditions of measurement. Accordingly, the comproportionation constants (K_C) of **1**−**3** are 4.09×10^5, 5.17×10^5, and 12.2×10^5, respectively. As per the Robin−Day classification,[49] the mixed-valence species of **1**−**3**, generated in situ, belong to class II. Thus, the presence of the hydroxide moiety as the bridging ligand effectively mediates metal−metal communication between the two Ir^{III} centers. In contrast to the dinuclear complexes, the monomers display a single oxidation peak, which is attributed to the metal center with a substantial contribution from the ligands (Figure 9).

dx.doi.org/10.1021/ic300694m | *Inorg. Chem.* 2012, 51, 10536−10547

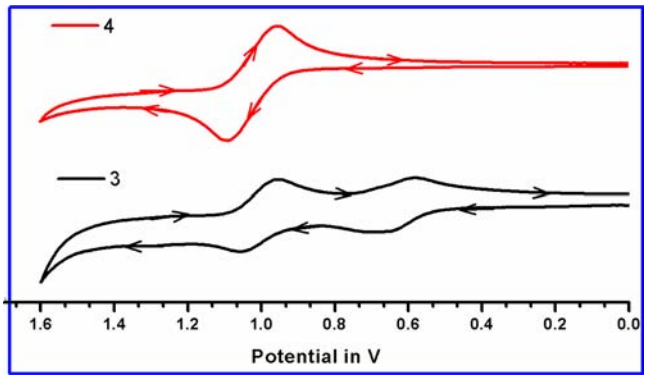

Figure 9. Cyclic voltammogram of dinuclear complex **3** and mononuclear complex **4**.

CONCLUSIONS

In this work, we report the first examples of heterobridged (pyrazole- and hydroxide-bridged) cyclometalated iridium(III) dimers. The hydroxide bridge results in a bathochromic shift of the (low-energy) absorption bands as well as the emission bands in comparison to the analogous mononuclear compounds. Additional insight into the photophysical behavior of these compounds was obtained by theoretical DFT and TDDFT calculations, which support the effect of the μ-OH ligand on the HOMO energy levels in the dinuclear compounds. Electrochemical studies reveal that the μ-OH ligand effectively mediates metal−metal communication in the dinuclear complexes.

EXPERIMENTAL SECTION

General Procedures. 2-Phenylpyridine (ppyH), 2-*p*-tolylpyridine (tpyH), dibenzoylmethane, and benzoylacetone were purchased from Aldrich Chemical Co. and were used as such without any further purification. Iridium chloride was purchased from Arora Matthey, Kolkata, India. Hydrazine hydrate was purchased from S.D. Fine Chemicals, Mumbai, India. Solvents were purified by conventional methods and were freshly distilled under a nitrogen atmosphere prior to use according to standard procedures. Sodium methoxide was freshly prepared and used in the reactions.

Instrumentation. ESI-HR mass analyses were performed on a Waters Micromass Quattro Micro triple-quadrupole mass spectrometer. ESI (positive ion, full scan mode) was carried out on solutions of **1** and **2** obtained by dissolving their crystals in acetonitrile containing 20% formic acid. Nitrogen gas was used for desolvation. The capillary voltage was maintained at 2.8 kV, and the cone voltage was kept at approximately 31 kV. ^{1}H NMR spectra were obtained on a JEOL-JNM Lambda 400 model and a JEOL-DELTA 2500 model NMR spectrometer using $CDCl_3$ as the solvent and tetramethylsilane $[Si(CH_3)_4]$ as the reference. NMR data are reported in ppm. Elemental analyses were carried out on fully dried samples using a Thermoquest CE Instruments CHNS-O, EA/110 model. IR spectra were recorded as KBr pellets in the range of 4000−400 cm^{-1} on a Bruker FT-IR Vector 22 model. UV−vis spectra were recorded on a Perkin-Elmer Lambda 20 UV−vis spectrometer in a 1×10^{-5} M dichloromethane solution. The steady-state emission spectra were measured using a Perkin-Elmer LS-55 model spectrophotometer in a 1×10^{-5} M dichloromethane solution. The lifetimes were measured by a time-correlated single-photon-counting spectrometer. The best fit was assessed based on the parameter χ^2, which was close to 1.0 for all of the samples. Quantum yields were measured with reference to $[Ir(ppy)_2(bpy)]PF_6$ (Φ_{CH_3CN} = 0.0622) using the following expression:

$$\Phi_S = \Phi_R(A_R/A_S)(I_S/I_R)(n_S^2/n_R^2)$$

In the above equation, the subscripts S and R denote sample and reference, respectively, Φ is the fluorescence quantum yield, A_S and A_R are the solution absorbances at the excitation wavelength, I_S and I_R are the integrated emission intensities, and n_S and n_R are the refractive indices of the solvent. All solvents were spectroscopic-grade, and deaerated solvents were prepared by the freeze−pump−thaw technique (repeated six times). Sample preparation was done in a drybox. Dilute solutions of compounds (OD < 0.1 at the excitation wavelength) were placed in quartz cuvettes fitted with Teflon stopcocks and then sealed before measurement.

Cyclic voltammetric studies were performed on a BAS Epsilon electrochemical workstation using a platinum working electrode, a Ag/AgCl reference electrode (3 M NaCl), and a platinum-wire counter electrode. All measurements were performed using 1 mM concentrations of the complexes in the presence of 0.1 M $[n\text{-}Bu_4N][PF_6]$ in dry dichloromethane. Comproportionation constants were calculated by using the equation $RT \ln K_C = nF(\Delta E)$, where ΔE corresponds to the difference between the first and second redox potentials in millivolts.[42]

X-ray Crystallography. Single crystals of **1**−**5** suitable for X-ray crystallography were obtained by the slow evaporation of their dichloromethane solutions, which have been layered with a few drops of methanol. X-ray data were collected on a CCD Bruker SMART APEX diffractometer at 100 K for **1**−**4** and at 293 K for **5** using a graphite-monochromated Mo Kα radiation (λ = 0.71073 Å). No decomposition of the crystals occurred during data collection. The program *SMART*[50] was used for collecting frames of data, indexing reflections, and determining lattice parameters, *SAINT* for integration of the intensity of reflections and scaling, *SADABS*[51] for absorption correction, and *SHELXTL*[52,53] for space-group and structure determination and least-squares refinements on F^2. All non-H atoms were refined with anisotropic displacement parameters. All H atoms except the −OH were fixed in geometrically calculated positions using a riding model and were refined isotropically. The −*OH* atoms for **1**−**3** and **5** were found from a difference Fourier map. The squeeze option in the *PLATON*[54] program was used to remove disordered solvent molecules (in **2**) from the overall intensity data of the compounds. The program package *ORTEP* was used for molecular graphics generation.

COMPUTATIONAL DETAILS

Gaussian03 was employed for all of the calculations.[55] The ground-state geometry of complex **1** was optimized by two different DFT methods: Becke's LYP (B3LYP) exchange correlational functional[56] and the gradient-corrected correlational functional PBE0.[57] However, hybrid PBE0 provided the best match with the geometrical X-ray data and was selected for our study (the main optimized geometry parameters for **1** at the B3LYP and PBE0 levels together with the experimental values given in Table S21, Supporting Information). Full geometry optimizations without symmetry constraints were carried out in the gas phase for the singlet ground state (S_0). The optimized geometry was confirmed to be the potential energy minima by vibrational frequency calculation at the same level of theory because no imaginary frequencies were found. In the calculation, the pseudopotential of the LANL2TZ basis set and a triple-ζ quality basis set LANL2TZ was adopted for Ir atoms, both of which were downloaded from the EMSL basis set library,[58] The D95V basis set was used on all of the nonmetal atoms. The orbital surfaces were visualized with *Gaussview*, and the percentage contributions of the metal atom and ligands to the respective orbitals were calculated using *Vmodes*.[59]

At the optimized geometry, TDDFT calculations were performed at the PBE0/LANL2DZ/D95 V level of theory in a dichloromethane solution by means of the PCM solvation model,[60] as implemented in the *Gaussian03* program package. The software *Gaussum*[61] was used for electronic spectrum simulation with fwhm = 0.4 eV. A total of 100 singlet−singlet excitations and the lowest 10 singlet−triplet excitations at the S_0-optimized geometry allowed us to simulate a large (up to 250 nm) portion of the absorption spectrum and gain insight into the nature of the transitions giving rise to the low-energy spectral region.

dx.doi.org/10.1021/ic300694m | *Inorg. Chem.* 2012, 51, 10536−10547

The oscillator strengths of singlet−triplet transitions are set to zero due to neglect of the spin−orbit coupling in the TDDFT calculations, so that these transitions do not contribute to the overall spectral profile.

For **4**, calculation at the PBE0/LANL2DZ/6-31G(d) level provided the best match with the geometrical X-ray data and was selected for our study (the main optimized geometry parameters for **4** at the B3LYP and PBE0 levels together with the experimental values given in Table S22, Supporting Information). In the calculations, the quasi-relativistic pseudopotentials of Ir atoms proposed by Hay and Wadt[62] with 17 valence electrons were used, and a double-ζ-quality basis set, LANL2DZ, was adopted. The 6-31G(d) basis set was used on all of the nonmetal atoms. At the optimized geometry, TDDFT calculations were performed at the PBE0/LANL2DZ/6-31G(d) level in a dichloromethane solution by means of the PCM solvation model,[60] as implemented in the *Gaussian03* program package. A total of 60 singlet−singlet excitations and the lowest 10 singlet−triplet excitations at the S_0-optimized geometry allowed us to simulate a large (up to 250 nm) portion of the absorption spectrum and gain insight into the nature of the transitions giving rise to the low-energy spectral region.

Synthesis. Complexes **1**−**5** were synthesized by a sequential two-step procedure. The cyclometalated chloro-bridged iridium(III) dimers $[(ppy)_2\,Ir(\mu\text{-}Cl)]_2$ (ppyH = 2-phenylpyridine) and $[(tpy)_2Ir\text{-}(\mu\text{-}Cl)]_2$ (tpyH = 2-*p*-tolylpyridine) were synthesized according to the Nonoyama route,[36] by refluxing $IrCl_3{\cdot}nH_2O$ with 2.5 equiv of the cyclometalating ligand (ppyH or tpyH) in a 3:1 mixture of 2-ethoxyethanol and water. The ligands Ph_2PzH and PhMePzH were synthesized following reported methods.[8,63] The detailed synthetic procedure is outlined below. All of the microanalytical data were obtained for compounds that were thoroughly dried under vacuum. During this process, the solvents of crystallization were completely lost.

$[(ppy)_2Ir(\mu\text{-}OH)(\mu\text{-}Ph_2Pz)Ir(ppy)_2]$ (1). In a 100 mL round-bottomed flask, $[(ppy)_2\,Ir(\mu\text{-}Cl)]_2$ (0.10 g, 0.093 mmol) was taken along with 30 mL of dichloromethane. To this was added solid sodium methoxide (0.025 g, 0.466 mmol), and the reaction mixture was allowed to stir at room temperature for about 2 h. At this point, the solution was orange in color. To this solution was added at once the ligand Ph_2PzH (0.086 g, 0.391 mmol), and the reaction mixture was continuously stirred at room temperature for 12 h. The progress of the reaction was monitored by thin-layer chromatography (TLC) by following the disappearance of $[(ppy)_2Ir(\mu\text{-}Cl)]_2$. [eluant: ethyl acetate/petroleum ether (60−80 °C; 20:80 (v/v)]. The reaction mixture was then filtered and the solvent removed in vacuo to afford an orange oil. To this was added diethyl ether (10 mL), and the solution was triturated, affording an orange solid. This was filtered and washed with cold methanol. The residue was recrystallized from dichloromethane by layering the solution with a few drops of methanol to give compound **1** as orange crystals. Yield: 0.077 g, 67%.

We could also isolate **1** in a reaction involving $[(ppy)_2Ir(\mu\text{-}Cl)]_2$ and Ph_2PzH in the presence of NaOH instead of NaOMe using a reaction procedure identical with that explained above. The quantities involved were $[(ppy)_2Ir(\mu\text{-}Cl)]_2$ (0.10 g, 0.093 mmol), sodium hydroxide (0.019 g, 0.466 mmol), Ph_2PzH (0.105 mmol, 0.023 g). Yield: 0.073 g, 64%.

Characterization Data. ESI-HRMS (80% acetonitrile, 20% formic acid): m/z 1236.2849 ($[M]^+$), 1219.2811 ($[M - OH]^+$). ^1H NMR (400 MHz, $CDCl_3$): Aromatic protons present in the compound were seen as a complex pattern. The centers of doublets and other multiplets are listed. δ 5.62 (d, J = 7.3 Hz, 2H), 5.74 (d, J = 7.08 Hz, 2H), 6.07 (s, 1H), 6.15−6.22 (m, 4H), 6.44 (d, J = 7.08 Hz, 4H), 6.45 (t, J = 7.2 Hz, 4H), 6.57−6.66 (m, 6H), 6.74−6.81 (m, 8H), 7.45−7.46 (m, 6H), 7.59−7.63 (m, 2H), 7.84 (d, J = 8.08 Hz, 2H), 8.23 (d, J = 5.6 Hz, 2H). IR (KBr, cm^{-1}): 3756(w), 3680(w), 3449(br), 3042(w), 2373(m), 1582(s), 1473(vs), 1419(m), 1264(w), 1159(w), 1030(w), 733(vs). Anal. Calcd for $C_{59}H_{44}Ir_2N_6O$: C, 57.27; H, 3.58; N, 6.79. Found; C, 57.14; H, 3.52; N, 6.82.

$[(tpy)_2Ir(\mu\text{-}OH)(\mu\text{-}Ph_2Pz)Ir(tpy)_2]$ (2). Using a procedure identical with that used for the preparation of **1**, compound **2** was obtained. The quantities involved were $[(tpy)_2Ir(\mu\text{-}Cl)]_2$ (0.10 g, 0.088 mmol), sodium methoxide (0.023 g, 0.44 mmol), and Ph_2PzH (0.105 mmol, 0.023 g). Yield: 0.071 g, 63%.

Characterization Data. ESI-HRMS (80% acetonitrile, 20% formic acid): m/z 1294.3485 ($[M]^+$), 1277.3444 ($[M - OH]^+$). ^1H NMR (400 MHz, $CDCl_3$): δ 1.75 (s, 6H), 1.82 (s, 6H), 5.39 (s, 2H), 5.56 (s, 2H), 6.00 (d, J = 6.84 Hz, 2H), 6.04 (s, 1H), 6.31 (d, J = 7.1 Hz, 4H), 6.37−6.41 (m, 2H), 6.46 (d, J = 6.8 Hz, 2H), 6.57−6.66 (m, 6H), 6.69−6.79 (m, 6H), 7.34−7.43 (m, 6H), 7.54−7.58 (m, 2H), 7.77 (d, J = 8.0 Hz, 2H), 8.19 (d, J = 5.4 Hz, 2H). IR (KBr, cm^{-1}): 3757(w), 3681(w), 3629(w), 3450(br, s), 3030(w), 2920(m), 2373(w), 1592(vs), 1469(vs), 1426(w), 1305(w), 1260(m), 1156(w), 1029(s), 804(w), 764(vs), 693(w), 493(w). Anal. Calcd for $C_{63}H_{52}Ir_2N_6O$: C, 58.50; H, 4.05; N, 6.50. Found; C, 58.62; H, 4.02; N, 6.58.

Synthesis of $[(ppy)_2Ir(\mu\text{-}OH)(\mu\text{-}PhMePz)Ir(ppy)_2]$ (3) and $[(ppy)_2Ir(PhMePz)Cl]$ (4). In a 100 mL round-bottomed flask, $[(ppy)_2Ir(\mu\text{-}Cl)]_2$ (0.30 g, 0.279 mmol) was taken along with 30 mL of dichloromethane. To this was added solid sodium methoxide (0.075 g, 1.398 mmol), and the reaction mixture was allowed to stir at room temperature for about 2 h. To this solution was added the ligand PhMePzH (0.066 g, 0.418 mmol), and the reaction mixture was continuously stirred at room temperature for 12 h. The progress of the reaction was monitored by TLC, which showed the formation of two products and the disappearance of $[(ppy)_2Ir(\mu\text{-}Cl)]_2$. [eluant: ethyl acetate/petroleum ether (60−80 °C; 20:80 (v/v))]. The reaction mixture was then filtered and the solvent removed in vacuo to afford an orange oil. To this was added diethyl ether (20 mL), and the solution was triturated, affording a yellowish-orange solid. This was filtered and washed with cold methanol. Further purification was achieved by column chromatography using an eluant mixture [eluant: ethyl acetate/petroleum ether (60−80 °C; 10:90 (v/v))], affording compounds **3** (orange in color) and **4** (yellow in color). Both compounds were then recrystallized from dichloromethane by layering their solutions with a few drops of methanol, affording **3** as orange crystals (yield: 0.118 g, 36%) and **4** as yellow crystals (yield: 0.054 g, 14%).

Complex **4** could also be prepared by another method in higher yields. ($[(ppy)_2Ir(\mu\text{-}Cl)]_2$ (0.10 g, 0.093 mmol) and PhMePzH (0.61 g, 0.39 mmol) in 30 mL of dichloromethane were stirred at room temperature for 12 h. The reaction mixture was filtered and the solvent evaporated in vacuo to afford a yellow oil. To this was added diethyl ether (10 mL), and the solution was triturated, affording a yellow solid. This was filtered and washed with methanol. The residue was recrystallized from dichloromethane by layering the solution with a few drops of methanol to give compound **4** as yellow crystals. Yield: 0.095 g, 74%.

Characterization Data for 3. ESI-HRMS (80% acetonitrile, 20% formic acid): m/z 1174.2694 ($[M]^+$), 1157.2598 ($[M - OH]^+$). ^1H NMR (400 MHz, $CDCl_3$): δ 1.18 (s, 3H), 5.57−5.62 (m, 2H), 5.71 (d, J = 7.8 Hz, 1H), 5.78 (s, 1H), 6.12−6.22 (m, 5H), 6.33−6.44 (m, 4H), 6.51−6.75 (m, 11H), 6.85 (d, J = 5.3 Hz, 1H), 7.40−7.53 (m, 8H), 7.62−7.77 (m, 3H), 7.89 (d, J = 7.8 Hz, 1H), 8.16 (dd, J_1 = 14.2 Hz, J_2 = 5.6 Hz, 1H). IR (KBr, cm^{-1}): 3448(br, s), 3036(w), 2923(s), 2853(w), 1602(s), 1580(s), 1560(w), 1474(s), 1437(w), 1413(s), 1302(w), 1265(w), 1223(w), 1158(w), 1059(w), 1029(m), 791(w), 753(vs), 728(w), 693(w), 629(w), 515(w). Anal. Calcd for $C_{54}H_{42}Ir_2N_6O$: C, 55.18; H, 3.60; N, 7.15. Found; C, 55.01; H, 3.7; N, 7.12.

Characterization Data for 4. ESI-HRMS (80% acetonitrile, 20% formic acid): m/z 659.1855 ($[M - Cl]^+$). ^1H NMR (500 MHz, $CDCl_3$): δ 1.37 (s, 3H), 6.16 (d, J = 6.7 Hz, 1H), 6.19 (s, 1H), 6.31 (d, J = 7.0 Hz, 2H), 6.68 (t, J = 6.8 Hz, 1H), 6.73 (t, J = 6.7 Hz, 1H), 6.82 (q, J = 7.4 Hz, 2H), 7.01 (t, J = 5.9 Hz, 1H), 7.33−7.36 (m, 1H), 7.41 (t, J = 7.5 Hz, 2H), 7.51 (d, J = 7.9 Hz, 1H), 7.55−7.58 (m, 3H), 7.66−7.72 (m, 2H), 7.78 (d, J = 7.9 Hz, 1H), 7.89 (d, J = 7.9 Hz, 1H), 8.08 (d, J = 4.8 Hz, 1H), 9.85 (d, J = 5.2 Hz, 1H), 13.69 (s, 1H). IR (KBr, cm^{-1}): 3100(w), 3035(w), 1604(s), 1581(s), 1562(s), 1476(vs), 1438(w), 1416(s), 1304(w), 1290(w), 1267(s), 1225(w), 1203(w), 1159(w), 1111(w), 1061(w), 1022(s), 960(w), 792(w), 756(vs), 729(s), 692(s), 669(w), 652(w), 629(w), 559(w). Anal. Calcd for

$C_{32}H_{26}ClIrN_4$: C, 55.36; H, 3.77; N, 8.07. Found; C, 55.31; H, 3.65; N, 8.15.

Synthesis of [(ppy)$_2$Ir(PhMePz)OH] (5). Complex **4** was used as the starting material for the synthesis. In a 100 mL round-bottomed flask, **4** (0.10 g, 0.144 mmol) was taken along with 30 mL of dichloromethane. To this was added solid sodium methoxide (0.038 g, 0.72 mmol), and the reaction mixture was allowed to stir at room temperature for about 2 h. To this solution was added the ligand PhMePzH (0.056 g, 0.360 mmol), and the reaction mixture was continuously stirred at room temperature for 12 h. The reaction mixture was then filtered and the solvent evaporated in vacuo to afford a yellow oil. To this was added diethyl ether (10 mL), and the solution was triturated, affording a yellow solid. This was filtered and washed with methanol. The residue was recrystallized from dichloromethane by layering the solution with a few drops of methanol to give compound **5** as yellow crystals. Yield: 0.060 g, 62%.

ESI-HRMS (80% acetonitrile, 20% formic acid): m/z 659.1677 ([M − OH]$^+$). ^{1}H NMR (500 MHz, $CDCl_3$): δ 1.37 (s, 3H), 6.16 (d, J = 7.6 Hz, 1H), 6.19 (s, 1H), 6.31 (d, J = 7.6 Hz, 2H), 6.68 (t, J = 7.3 Hz, 1H), 6.73 (t, J = 7.3 Hz, 1H), 6.82 (q, J = 7.7 Hz, 2H), 7.01 (t, J = 6.5 Hz, 1H), 7.14 (d, J = 6.5 Hz, 1H), 7.33−7.36 (m, 1H), 7.41 (t, J = 7.8 Hz, 2H), 7.51 (d, J = 7.3 Hz, 1H), 7.55−7.58 (m, 3H), 7.66−7.72 (m, 2H), 7.78 (d, J = 7.9 Hz, 1H), 7.89 (d, J = 7.9 Hz, 1H), 8.08 (d, J = 5.1 Hz, 1H), 9.85 (d, J = 5.2 Hz, 1H). IR (KBr, cm^{-1}): 3442(br, s), 3037(w). 2923(w), 1603(s), 1581(s), 1476(vs), 1438(w), 1416(s), 1304(w), 1267(s), 1225(w), 1204(w), 1160(w), 1061(w), 1029(s), 793(w), 755(vs), 731(s), 693(w), 670(w), 630(w), 558(w). Anal. Calcd for $C_{32}H_{27}IrN_4O$: C, 56.87; H, 4.03; N, 8.29. Found; C, 56.58; H, 4.06; N, 8.23.

■ ASSOCIATED CONTENT

Supporting Information

X-ray crystallographic data for compounds **1**−**5** in CIF format, molecular orbital diagrams of **2**, **3**, and **5**, emission spectra of **1**−**5** in different solvents, bond distance and angle data for **1**−**5**, tables summarizing theoretical analysis on **1**, **4**, and **5**, and the optimized coordinates for **1**−**5**. This material is available free of charge via the Internet at http://pubs.acs.org.

■ AUTHOR INFORMATION

Corresponding Author

*E-mail: vc@iitk.ac.in (V.C.), bhanu2505@yahoo.co.in (K.B.). Phone: (+91) 512-259-7259. Fax: (+91) 521-259-0007/7436.

Notes

The authors declare no competing financial interest.

■ ACKNOWLEDGMENTS

We thank the Department of Science and Technology (DST), India, for financial support. B.M. and P.B. are thankful to CSIR, New Delhi, India, for fellowships. We also thank Dr. Raghumani Singh Ningthoujam (Scientist, Structural Chemistry Division, Bhabha Atomic Research Centre, Mumbai, India) for his help in lifetime studies and Dr. L. Nagarajan and Dr. K. Gopal for valuable suggestions during the manuscript preparation. We also thank Dr. Pratik Sen (IIT Kanpur) for valuable discussions.

■ REFERENCES

(1) Halcrow, M. A. *Dalton Trans.* **2009**, 2059−2073.
(2) Klingele, J.; Dechert, S.; Meyer, F. *Coord. Chem. Rev.* **2009**, *253*, 2698−2741.
(3) Mukherjee, R. *Coord. Chem. Rev.* **2000**, *203*, 151−218.
(4) Viciano-Chumillas, M.; Tanase, S.; de Jongh, L. J.; Reedijk, J. *Eur. J. Inorg. Chem.* **2010**, 3403−3418.
(5) Dias, H. V. R.; Diyabalanage, H. V. K.; Eldabaja, M. G.; Elbjeirami, O.; Rawashdeh-Omary, M. A.; Omary, M. A. *J. Am. Chem. Soc.* **2005**, *127*, 7489−7501.
(6) Casarin, M.; Cingolani, A.; Di Nicola, C.; Falcomer, D.; Monari, M.; Pandolfo, L.; Pettinari, C. *Cryst. Growth Des.* **2007**, *7*, 676−685.
(7) Mezei, G.; Raptis, R. G. *Inorg. Chim. Acta* **2004**, *357*, 3279−3288.
(8) Mezei, G.; Rivera-Carrillo, M.; Raptis, R. G. *Inorg. Chim. Acta* **2004**, *357*, 3721−3732.
(9) Mezei, G.; Rivera-Carrillo, M.; Raptis, R. G. *Dalton Trans.* **2007**, 37−40.
(10) Chandrasekhar, V.; Thilagar, P.; Murugesa Pandian, B. *Coord. Chem. Rev.* **2007**, *251*, 1045−1074.
(11) Van der Vlugt, J. I.; Demeshko, S.; Dechert, S.; Meyer, F. *Inorg. Chem.* **2008**, *47*, 1576−1585.
(12) Chandrasekhar, V.; Thirumoorthi, R. *Organometallics* **2009**, *28*, 2096−2106.
(13) Chandrasekhar, V.; Thirumoorthi, R.; Azhakar, R. *Organometallics* **2007**, *26*, 26−29.
(14) Baldo, M. A.; O'Brien, D. F.; You, Y.; Shoustikov, A.; Sibley, S.; Thompson, M. E.; Forrest, S. R. *Nature* **1998**, *395*, 151−154.
(15) Baldo, M. A.; Thompson, M. E.; Forrest, S. R. *Nature* **2000**, *403*, 750−753.
(16) Chou, P.-T.; Chi, Y. *Chem.—Eur. J.* **2007**, *13*, 380−395.
(17) Holder, E.; Langeveld, B. M. W.; Schubert, U. S. *Adv. Mater.* **2005**, *17*, 1109−1121.
(18) Andreiadis, E. S.; Imbert, D.; Pécaut, J.; Calborean, A.; Ciofini, I.; Adamo, C.; Demadrille, R.; Mazzanti, M. *Inorg. Chem.* **2011**, *50*, 8197−8206.
(19) Auffrant, A.; Barbieri, A.; Barigelletti, F.; Collin, J.-P.; Flamigni, L.; Sabatini, C.; Sauvage, J.-P. *Inorg. Chem.* **2006**, *45*, 10990−10997.
(20) Auffrant, A.; Barbieri, A.; Barigelletti, F.; Lacour, J.; Mobian, P.; Collin, J.-P.; Sauvage, J.-P.; Ventura, B. *Inorg. Chem.* **2007**, *46*, 6911−6919.
(21) Baranoff, E.; Orselli, E.; Allouche, L.; Di Censo, D.; Scopelliti, R.; Gratzel, M.; Nazeeruddin, M. K. *Chem.Commun.* **2011**, *47*, 2799−2801.
(22) Bettington, S.; Tavasli, M.; Bryce, M. R.; Batsanov, A. S.; Thompson, A. L.; Al Attar, H. A.; Dias, F. B.; Monkman, A. P. *J. Mater. Chem.* **2006**, *16*, 1046−1052.
(23) Chandrasekhar, V.; Wahidur Rahaman, S. M.; Hajra, T.; Das, D.; Ghatak, T.; Rafiq, S.; Sen, P.; Bera, J. K. *Chem. Commun.* **2011**, *47*, 10836−10838.
(24) Costa, R. D.; Fernández, G.; Sánchez, L.; Martín, N.; Ortí, E.; Bolink, H. J. *Chem.—Eur. J.* **2010**, *16*, 9855−9863.
(25) Fernández-Hernández, J. M.; Yang, C.-H.; Beltrán, J. I.; Lemaur, V.; Polo, F.; Fröhlich, R.; Cornil, J.; De Cola, L. *J. Am. Chem. Soc.* **2011**, *133*, 10543−10558.
(26) Lafolet, F.; Welter, S.; Popovic, Z.; Cola, L. D. *J. Mater. Chem.* **2005**, *15*, 2820−2828.
(27) Plummer, E. A.; Hofstraat, J. W.; De Cola, L. *Dalton Trans.* **2003**, 2080−2084.
(28) Tsuboyama, A.; Takiguchi, T.; Okada, S.; Osawa, M.; Hoshino, M.; Ueno, K. *Dalton Trans.* **2004**, 1115−1116.
(29) Zheng, Y.; Batsanov, A. S.; Bryce, M. R. *Inorg. Chem.* **2011**, *50*, 3354−3362.
(30) Hajra, T.; Bera, J. K.; Chandrasekhar, V. *Inorg. Chim. Acta* **2011**, *372*, 53−61.
(31) Hajra, T.; Bera, J. K.; Chandrasekhar, V. *Aust. J. Chem.* **2011**, *64*, 561−566.
(32) Chandrasekhar, V.; Hajra, T.; Bera, J. K.; Rahaman, S. M. W.; Satumtira, N.; Elbjeirami, O.; Omary, M. A. *Inorg. Chem.* **2012**, *51*, 1319−1329.
(33) Hajra, T.; Ghosh, S.; Bera, J. K.; Chandrasekhar, V. *Indian J. Chem.* **2011**, *50A*, 1290−1297.
(34) Li, J.; Djurovich, P. I.; Alleyne, B. D.; Tsyba, I.; Ho, N. N.; Bau, R.; Thompson, M. E. *Polyhedron* **2004**, *23*, 419−428.
(35) Li, J.; Djurovich, P. I.; Alleyne, B. D.; Yousufuddin, M.; Ho, N. N.; Thomas, J. C.; Peters, J. C.; Bau, R.; Thompson, M. E. *Inorg. Chem.* **2005**, *44*, 1713−1727.

(36) Nonoyama, M. *Bull. Chem. Soc. Jpn.* **1974**, *47*, 767−768.
(37) Yuan, X.; Zhang, S.; Ding, Y. *Inorg. Chem. Commun.* **2012**, *17*, 26−29.
(38) Ionkin, A. S.; Wang, Y.; Marshall, W. J.; Petrov, V. A. *J. Organomet. Chem.* **2007**, *692*, 4809−4827.
(39) Bushnell, G. W.; Fjeldsted, D. O. K.; Stobart, S. R.; Zaworotko, M. J.; Knox, S. A. R.; MacPherson, K. A. *Organometallics* **1985**, *4*, 1107−1114.
(40) Tejel, C.; Ciriano, M. A.; Millaruelo, M.; López, J. A.; Lahoz, F. J.; Oro, L. A. *Inorg. Chem.* **2003**, *42*, 4750−4758.
(41) Bardwell, D. A.; Horsburgh, L.; Jeffery, J. C.; Joulie, L. F.; Ward, M. D.; Webster, I.; Yellowlees, L. J. *J. Chem. Soc., Dalton Trans.* **1996**, 2527−2531.
(42) Jude, H.; Rein, F. N.; White, P. S.; Dattelbaum, D. M.; Rocha, R. C. *Inorg. Chem.* **2008**, *47*, 7695−7702.
(43) Beeby, A.; Bettington, S.; Samuel, I. D. W.; Wang, Z. *J. Mater. Chem.* **2003**, *13*, 80−83.
(44) Edkins, R. M.; Wriglesworth, A.; Fucke, K.; Bettington, S. L.; Beeby, A. *Dalton Trans.* **2011**, *40*, 9672−9678.
(45) Goldsmith, J. I.; Hudson, W. R.; Lowry, M. S.; Anderson, T. H.; Bernhard, S. *J. Am. Chem. Soc.* **2005**, *127*, 7502−7510.
(46) Costa, R.; Monti, F.; Accorsi, G.; Barbieri, A.; Bolink, H. J.; Ortí, E.; Armaroli, N. *Inorg. Chem.* **2011**, *50*, 7229−7238.
(47) Di Censo, D.; Fantacci, S.; De Angelis, F.; Klein, C.; Evans, N.; Kalyanasundaram, K.; Bolink, H. J.; Gratzel, M.; Nazeeruddin, M. K. *Inorg. Chem.* **2008**, *47*, 980−989.
(48) Hay, P. J. *J. Phys. Chem. A* **2002**, *106*, 1634−1641.
(49) Robin, M. B.; Day, P. *Adv. Inorg. Chem. Radiochem.* **1967**, *10*, 247.
(50) *SMART & SAINT Software Reference Manuals*, version 6.45; Bruker Analytical X-ray Systems, Inc.: Madison, WI, 2003.
(51) Sheldrick, G. M. *SADABS, a software for empirical absorption correction*, version 2.05; University of Göttingen: Göttingen, Germany, 2002.
(52) Sheldrick, G. M. *SHELXTL*, version 6.12; Bruker Analytical X-ray Systems, Inc.: Madison, WI, 2001.
(53) Sheldrick, G. M. *SHELXTL Reference Manual*, version 6.1; Bruker Analytical X-ray Systems, Inc.: Madison, WI, 2000.
(54) Spek, A. L. *PLATON*; University of Utrecht: Utrecht, The Netherlands, 2001.
(55) Frisch, M. J.; Trucks, G. W.; Schlegel, H. B.; Scuseria, G. E.; Robb, M. A.; Cheeseman, J. R.; Montgomery, J. A.; Vreven, T.; Kudin, K. N.; Burant, J. C.; Millam, J. M.; Iyengar, S. S.; Tomasi, J.; Barone, V.; Mennucci, B.; Cossi, M.; Scalmani, G.; Rega, N.; Petersson, G. A.; Nakatsuji, H.; Hada, M.; Ehara, M.; Toyota, K.; Fukuda, R.; Hasegawa, J.; Ishida, M.; Nakajima, T.; Honda, Y.; Kitao, O.; Nakai, H.; Klene, M.; Li, X.; Knox, J. E.; Hratchian, H. P.; Cross, J. B.; Adamo, C.; Jaramillo, J.; Gomperts, R.; Stratmann, R. E.; Yazyev, O.; Austin, A. J.; Cammi, R.; Pomelli, C.; Ochterski, J. W.; Ayala, P. Y.; Morokuma, K.; Voth, G. A.; Salvador, P.; Dannenberg, J. J.; Zakrzewski, V. G.; Dapprich, S.; Daniels, A. D.; Strain, M. C.; Farkas, O.; Malick, D. K.; Rabuck, A. D.; Raghavachari, K.; Foresman, J. B.; Ortiz, J. V.; Cui, Q.; Baboul, A. G.; Clifford, S.; Cioslowski, J.; Stefanov, B. B.; Liu, G.; Liashenko, A.; Piskorz, P.; Komaromi, I.; Martin, R. L.; Fox, D. J.; Keith, T.; Al-Laham, M. A.; Peng, C. Y.; Nanayakkara, A.; Challacombe, M.; Gill, P. M. W.; Johnson, B.; Chen, W.; Wong, M. W.; Gonzalez, C.; Pople, J. A. *Gaussian03*; Gaussian, Inc.: Wallingford, CT, 2003.
(56) Lee, C.; Yang, W.; Parr, R. G. *Phys. Rev. B* **1988**, *37*, 785−789.
(57) Perdew, J. P.; Burke, K.; Ernerhof, M. *Phys. Rev. Lett.* **1997**, *78*, 1396.
(58) Schuchardt, K. L.; Didier, B. T.; Elsethagen, T.; Sun, L.; Gurumoorthi, V.; Chase, J.; Li, J.; Windus, T. L. *J. Chem. Inf. Model.* **2007**, *47*, 1045−1052.
(59) Nemykin, V. N.; Basu, P. *VMOdes Program*, revision A7.2; University of Minnesota, Duluth: Duluth, MN, 2001.
(60) Cossi, M.; Scalmani, G.; Regar, N.; Barone, V. *J. Chem. Phys.* **2002**, *117*, 43−54.
(61) O'Boyle, N. M.; Tenderholt, A. L. *J. Comput. Chem.* **2008**, *29*, 839−845.
(62) Hay, P. J.; Wadt, W. R. *J. Chem. Phys.* **1985**, *82*, 299−310.
(63) Kitajima, N.; Fujisawa, K.; Fujimoto, C.; Morooka, Y.; Hashimoto, S.; Kitagawa, T.; Toriumi, K.; Tatsumi, K.; Nakamura, A. *J. Am. Chem. Soc.* **1992**, *114*, 1277−1291.